Supplementary Information

Rydberg Atom Sensors Enable High-Resolution Terahertz Frequency Detection and Precision Spectroscopy

CONTENTS

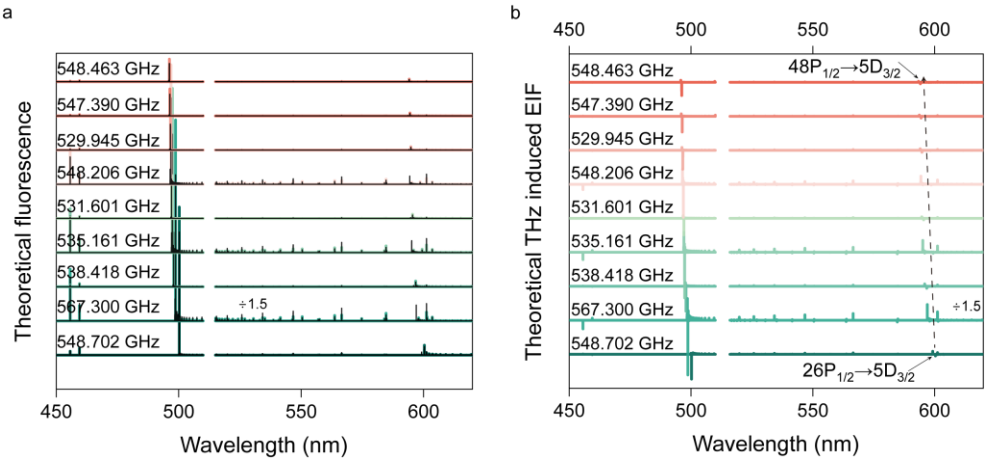

Fig. S1. (a) Theoretical fluorescence spectra of cesium atoms without (colored) and with (black) a THz field in the 450–620 nm range. Theoretical THz transition channels $n_1R_{a/b} \rightarrow n_2R_{c/d}$ include: $24D_{3/2} \rightarrow 26P_{1/2}$ (548.702 GHz), $29S_{1/2} \rightarrow 30P_{1/2}$ (567.300 GHz), $30D_{3/2} \rightarrow 33P_{1/2}$ (538.418 GHz), $34S_{1/2} \rightarrow 36P_{1/2}$ (535.161 GHz), $34D_{3/2} \rightarrow 38P_{1/2}$ (531.601 GHz), $37S_{1/2} \rightarrow 40P_{1/2}$ (548.206 GHz), $37D_{3/2} \rightarrow 42P_{1/2}$ (529.945 GHz), $39D_{3/2} \rightarrow 45P_{1/2}$ (537.399 GHz), and $41D_{3/2} \rightarrow 48P_{1/2}$ (547.463 GHz), respectively. (b) Theoretical THz-induced EIF spectra with nine distinct THz frequencies.

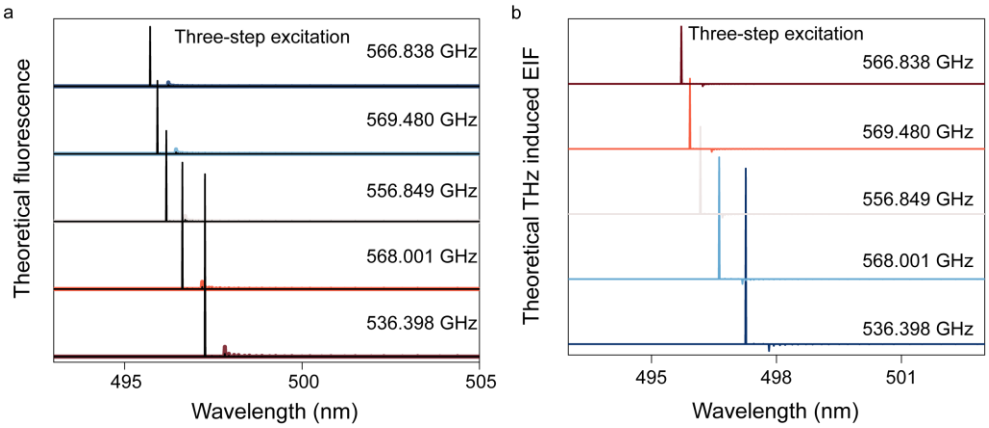

Fig. S2 (a) Theoretical fluorescence spectra of cesium atoms without (colored) and with (black) a THz field by three-step excitation. The THz transition channels $n_1R_{a/b} \rightarrow n_2R_{c/d}$ include: $32P_{3/2} \rightarrow 33D_{3/2}$ (536.398 GHz), $35P_{3/2} \rightarrow 37D_{3/2}$ (568.001 GHz), $38P_{3/2} \rightarrow 41D_{3/2}$ (556.849 GHz), $40P_{3/2} \rightarrow 44D_{3/2}$ (569.480 GHz), and $42P_{3/2} \rightarrow 47D_{3/2}$ (566.838 GHz). (b) Theoretical THz-induced EIF spectra corresponding to the THz frequencies.

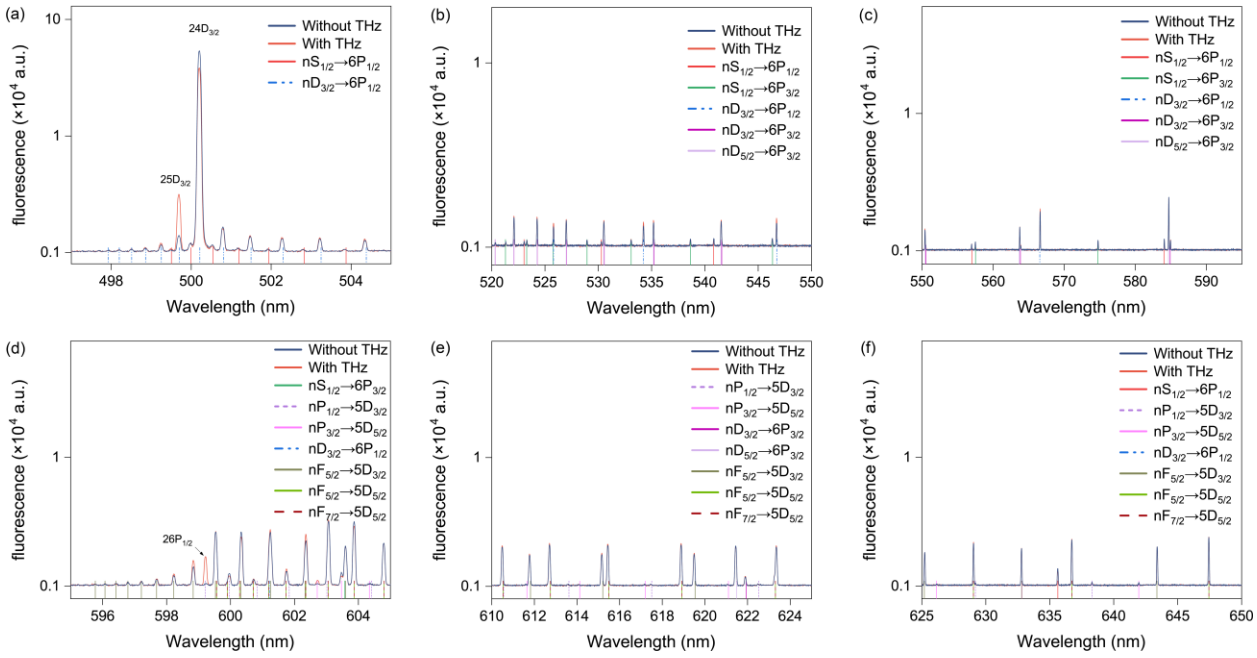

Fig. S3. Theoretical decay channels and experimental fluorescence spectra of the $24D_{3/2}$ and $26P_{1/2}$ states. Experimental fluorescence spectra are shown for the wavelength ranges of (a) 495–505 nm, (b) 520–550 nm, (c) 550–595 nm, (d) 595–605 nm, (e) 610–625 nm, and (f) 625–650 nm. Vertical lines indicate the theoretically predicted decay channels.

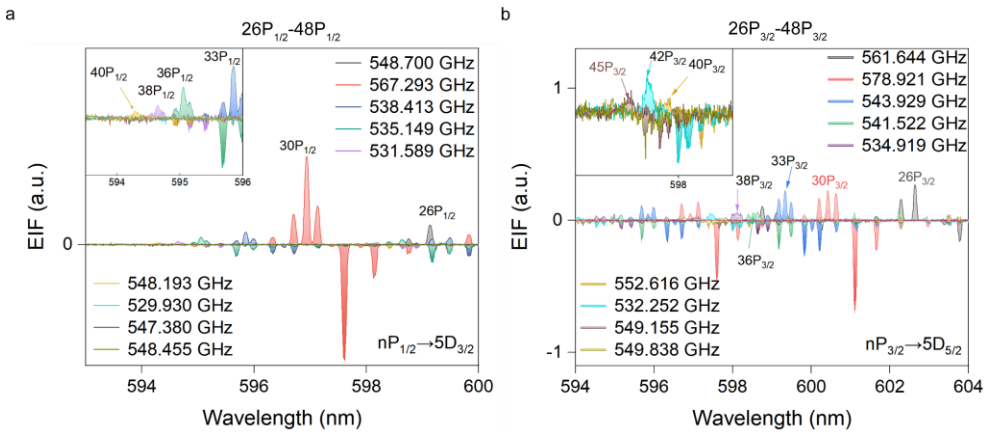

Fig. S4 (a) THz-induced EIF spectra for the $26P_{1/2}$–$48P_{1/2}$ state, covering the wavelength range of 593–600 nm. Experimental THz frequencies correspond to the following atomic transitions: $24D_{3/2} \rightarrow 26P_{1/2}$ (548.700 GHz), $29S_{1/2} \rightarrow 30P_{1/2}$ (546.293 GHz), $30D_{3/2} \rightarrow 33P_{1/2}$ (538.413 GHz), $34S_{1/2} \rightarrow 36P_{1/2}$ (535.149 GHz), $34D_{3/2} \rightarrow 38P_{1/2}$ (531.589 GHz), $37S_{1/2} \rightarrow 40P_{1/2}$ (548.193 GHz), $37D_{3/2} \rightarrow 42P_{1/2}$ (529.930 GHz), $39D_{3/2} \rightarrow 45P_{1/2}$ (547.380 GHz), $41D_{3/2} \rightarrow 48P_{1/2}$ (548.455 GHz). (b) THz-induced EIF spectra for the $26P_{3/2}$–$48P_{3/2}$ state, covering the wavelength range of 594–604 nm. Experimental THz frequencies correspond to the following atomic transitions: $24D_{5/2} \rightarrow 26P_{3/2}$ (561.644 GHz), $29S_{1/2} \rightarrow 30P_{3/2}$ (578.921 GHz), $30D_{5/2} \rightarrow 33P_{3/2}$ (543.929 GHz), $34S_{1/2} \rightarrow 36P_{3/2}$ (541.522 GHz), $34D_{5/2} \rightarrow 38P_{3/2}$ (534.919 GHz), $37S_{1/2} \rightarrow 40P_{3/2}$ (552.616 GHz), $37D_{5/2} \rightarrow 42P_{3/2}$ (532.252 GHz), $39D_{5/2} \rightarrow 45P_{3/2}$ (549.155 GHz), $41D_{5/2} \rightarrow 48P_{3/2}$ (549.838 GHz).

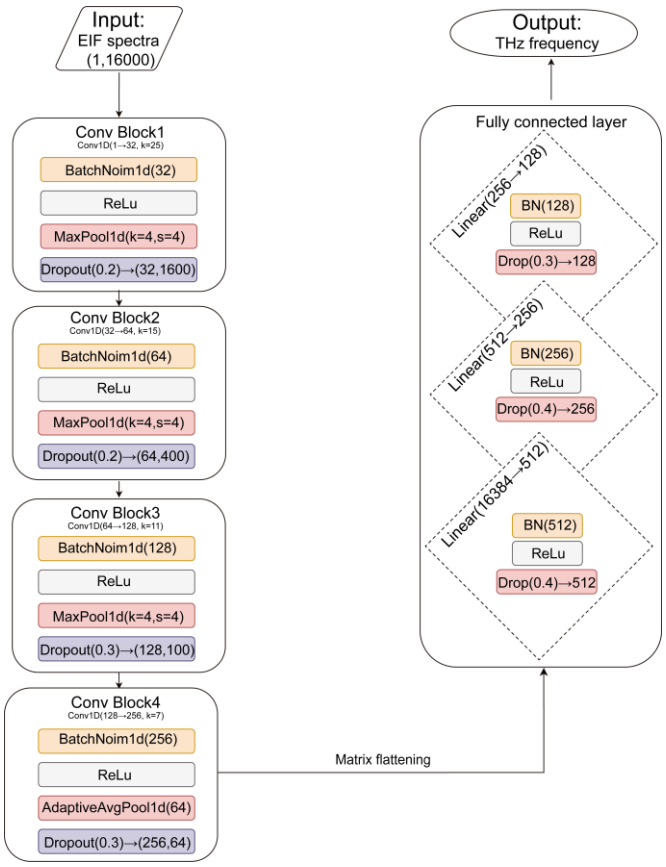

Fig. S5: Structure of the deep learning model. The model comprises four 1D-CNN, which consists of four sublayers: Batch Normalization, ReLU activation, MaxPooling1D, and Dropout. Following these convolutional layers, a fully connected layer classifies the EIF spectra and outputs the predicted THz frequency.

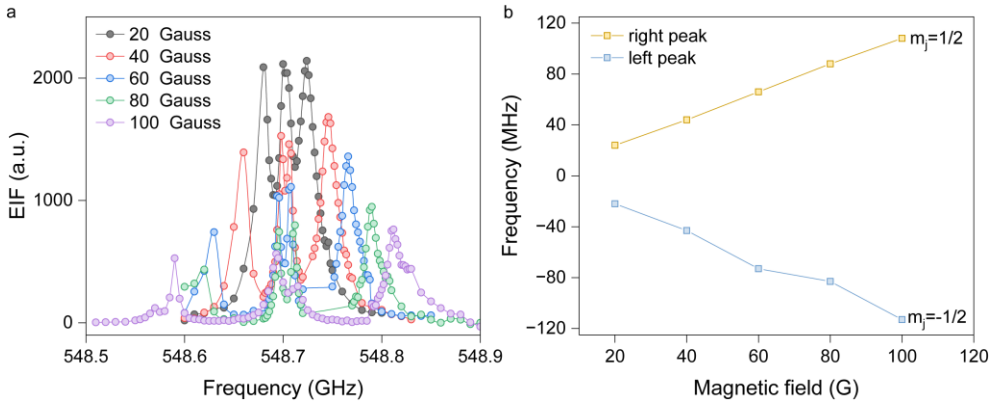

Fig. S6 (a) Detuning of THz-induced EIF peak at 499.6 nm measured under magnetic fields ranging from 20 to 100 Gs. (b) Frequency shift of EIF spectral peak in the 20–100 Gs magnetic field range.

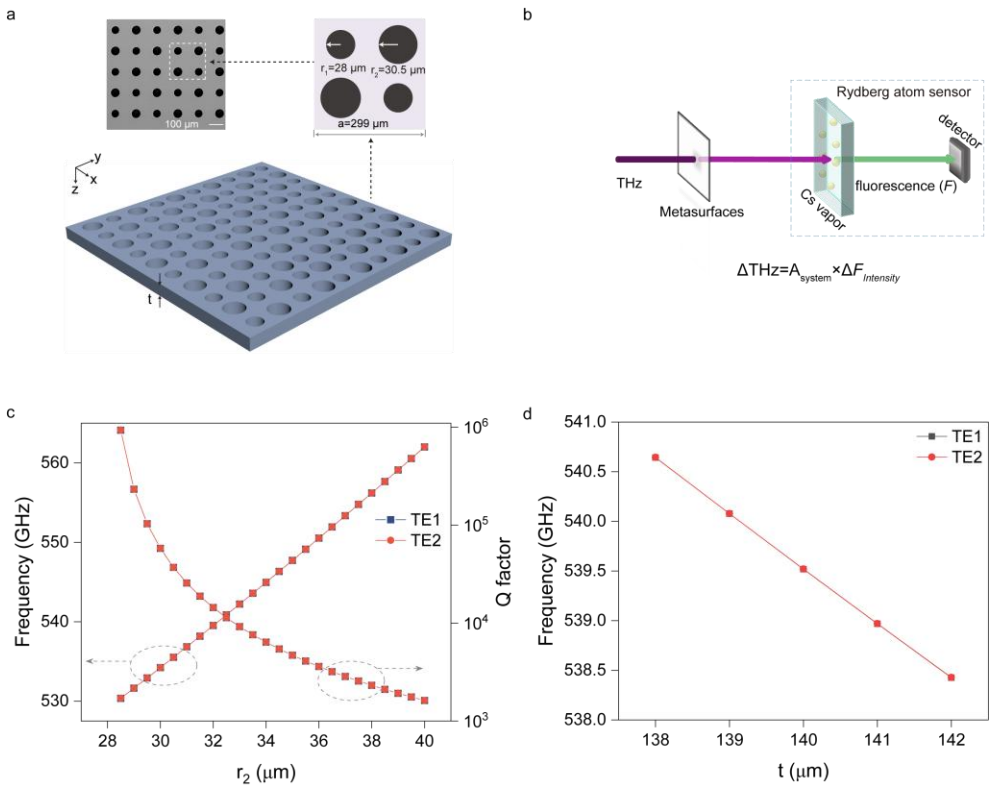

Fig. S7 (a) SEM images of the fabricated metasurfacesand a schematic of a periodic air-porous all-silicon THz metasurface. (b) Schematic of Rydberg atom sensor to characterize THz metasurfaces, featuring a divergent THz beam is used in the measurement system. (c) Simulated resonance frequencies and Q factors of the TE1 and TE2 modes of the THz metasurface for r_1 = 28 μm, r_2 = 28–40 μm, and a = 306 μm. (d) Simulated resonance frequencies of the TE1 and TE2 modes of the THz metasurface for r_1 = 28 μm, r_2 = 32 μm, and a = 306 μm with varyingwafer thicknesses t.

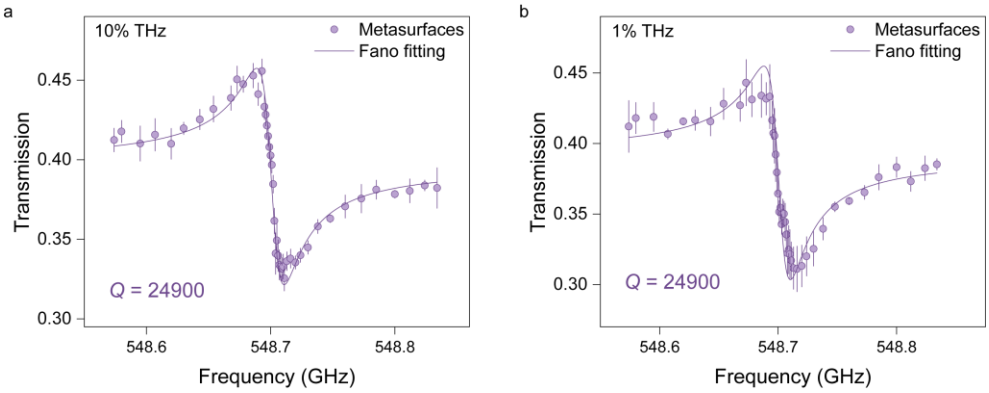

Fig. S8 The Rydberg-atom sensor measures the THz transmission spectra of the metasurface at (a) 10% and (b) 1% of the rated THz power.

Tables

Table 1 Initial Rydberg states $n_1R_{a/b}$, final Rydberg states $n_2R_{1/2}$, coupling laser wavelengths, dipole moments, and corresponding THz frequencies from two-step excitation.

Energy level	Coupling laser (nm)	Transition dipole moment	$n_1R_{a/b}$	THz field (GHz)	Transition dipole moment	$n_2P_{1/2}$
$6P_{3/2}$	514.4746	0.1154	$24D_{3/2}$	548.702	219.903	$26P_{1/2}$
	512.8763	0.0406	$29S_{1/2}$	567.300	81.601	$30P_{1/2}$
	512.0508	0.0792	$30D_{3/2}$	546.837	103.496	$33P_{1/2}$
	511.4612	0.0307	$34S_{1/2}$	535.161	45.791	$36P_{1/2}$
	511.1498	0.0644	$34D_{3/2}$	531.601	75.095	$38P_{1/2}$
	510.9055	0.0266	$37S_{1/2}$	548.206	30.523	$40P_{1/2}$
	510.6701	0.0561	$37D_{3/2}$	529.945	56.651	$42P_{1/2}$
	510.4150	0.0515	$39D_{3/2}$	547.390	44.435	$45P_{1/2}$
	510.1983	0.0475	$41D_{3/2}$	548.463	37.055	$48P_{1/2}$

Table 2 Initial Rydberg states $n_1R_{a/b}$, final Rydberg states $n_2R_{c/d}$, coupling laser wavelengths, dipole moments, and corresponding THz frequencies from three-step excitation.

Energy level	Coupling laser (nm)	Transition dipole moment	$n_1R_{a/b}$	THz field (GHz)	Transition dipole moment	$n_2D_{3/2}$
$7S_{1/2}$	785.2208	0.02252	$32P_{3/2}$	536.398	80.0168	$33D_{3/2}$
	783.7035	0.01927	$35P_{3/2}$	568.000	54.6554	$37D_{3/2}$
	782.5691	0.01674	$38P_{3/2}$	556.849	42.8612	$41D_{3/2}$
	781.9647	0.01538	$40P_{3/2}$	569.479	34.5032	$47D_{3/2}$
	781.4829	0.01414	$42P_{3/2}$	566.838	29.1419	$47D_{3/2}$

Table 3 Initial Rydberg states $n_1R_{a/b}$, final Rydberg states $n_2R_{3/2}$, coupling laser wavelengths, dipole moments, and corresponding THz frequencies from two-step excitation.

Energy level	Coupling laser (nm)	Transition dipole moment	$n_1R_{a/b}$	THz field (GHz)	Transition dipole moment	$n_2R_{3/2}$
$6P_{3/2}$	514.4693	0.1151	$24D_{5/2}$	561.689	203.214	$26P_{3/2}$
	512.8763	0.0406	$29S_{1/2}$	578.921	91.749	$30P_{3/2}$
	512.0483	0.0790	$30D_{5/2}$	543.956	105.783	$33P_{3/2}$
	511.4612	0.0307	$34S_{1/2}$	541.454	53.480	$36P_{3/2}$
	511.1481	0.0643	$34D_{5/2}$	534.941	72.145	$38P_{3/2}$
	510.9055	0.0266	$37S_{1/2}$	552.645	36.319	$40P_{3/2}$
	510.6693	0.0560	$37D_{5/2}$	532.266	54.681	$42P_{3/2}$
	510.4139	0.0514	$39D_{5/2}$	549.175	43.001	$45P_{3/2}$
	510.1974	0.0474	$41D_{5/2}$	549.859	35.932	$48P_{3/2}$